Sedimentation

Sedimentation

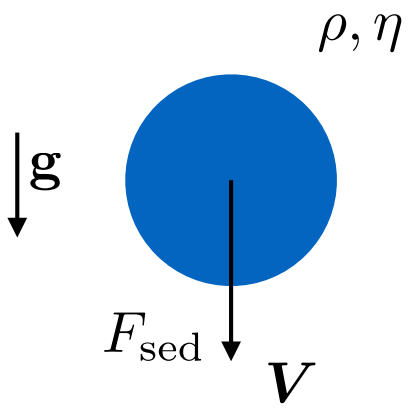

$$\boldsymbol{F}_g = \frac{4}{3}\pi\rho_p a^3 \boldsymbol{g}$$ Gravity

$$\boldsymbol{F}_b = -\frac{4}{3}\pi\rho_f a^3 \boldsymbol{g}$$ Buoyancy

$$\boldsymbol{F}_{\text{sed}} = \frac{4}{3}\pi a^3 \Delta\rho \boldsymbol{g}$$

$$\frac{4}{3}\pi a^3 \Delta\rho \boldsymbol{g} - \zeta \boldsymbol{V} = 0$$ Equation of motion (neglecting inertia)

$$\boldsymbol{V} = \frac{2\pi a^2 \Delta\rho \boldsymbol{g}}{9\eta_s}$$

Gravitational Peclet number

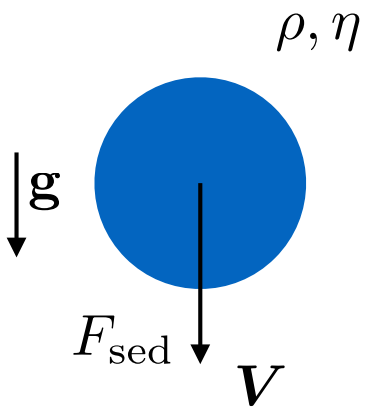

$$\mathrm{Pe}_g = t_B / t_{\text{sed}} = \frac{4\pi^2 a^4 \Delta\rho g}{kT}$$

with $$t_{\text{sed}} = \frac{9\eta_s}{2\pi a \Delta\rho g}$$

$\mathrm{Pe}_g \ll 1$ particles stay dispersed by Brownian motion

$\mathrm{Pe}_g \gg 1$ particles sediment rapidly

Equilibrium and the gravitational length

What is the probability that a particle will be at a height z?

$$U_g = mgz = V_p \Delta\rho g z = \frac{4}{3}\pi a^3 \Delta\rho g z$$

Gravitational energy in a gravitational field

$$p(z) = \frac{e^{-U_g/kT}}{\int_0^\infty e^{-U_g/kT} dz}$$

$$= \frac{mg}{kT} e^{-mgz/kT}$$

$$= \frac{4\pi a^3 \Delta\rho g}{3kT} e^{-4\pi a^3 \Delta\rho g z/3kT}$$

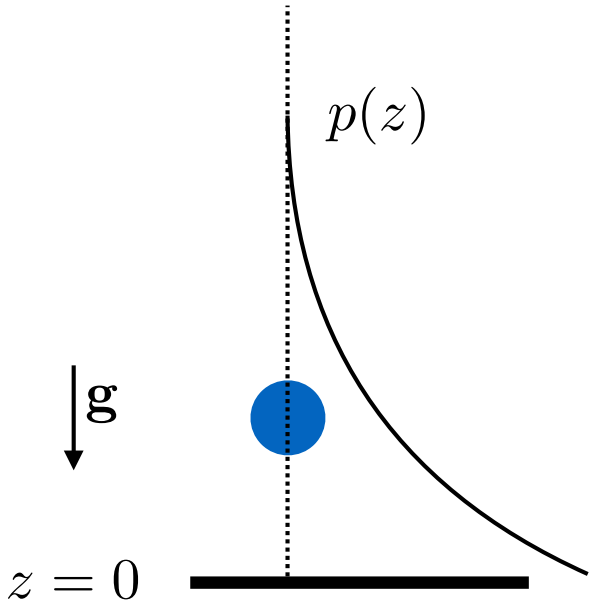

$$l_g = \frac{3kT}{4\pi a^3 \Delta\rho g}$$

Gravitational length

Diffusion and settling

What is the probability that a particle will be at a height z?

$$j_{\text{sed}} = -Vn(z)$$ flux due to sedimentation

$$j_{\text{diff}} = -D_0 \frac{dn}{dz}$$ balanced by diffusion at equilibrium

$$j_{\text{sed}} + j_{\text{diff}} = 0$$

$$n(z) = C \exp\left(\frac{-Vz}{D_0}\right)$$

$$D_0/V = \frac{kT}{6\pi a \eta_s} \cdot \frac{9\eta_s}{2\pi a^2 \Delta\rho g} = \frac{3kT}{4\pi^2 a^3 \Delta\rho g} = l_g$$

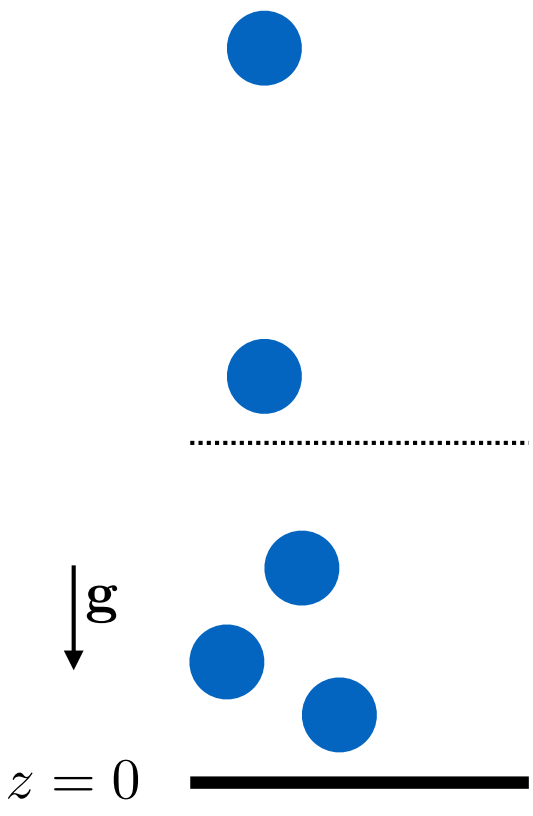

$$n(z) = \frac{n_0 V h}{D_0} \frac{\exp(-Vz/D_0)}{1 - \exp(-Vh/D_0)}$$

Like energy earlier, but finite height of column

Higher concentrations

Particle concentration (osmotic pressure) and hydrodynamic interactions (settling dynamics and diffusion) will play a role

Davis, K. E.; Russel, W. B. *J. Chem. Soc. Faraday Trans.* 1991, 87, 411–424.
Davis, K. E.; Russel, W. B. *Phys. Fluids A Fluid Dyn.* 1989, 82, 82–100.

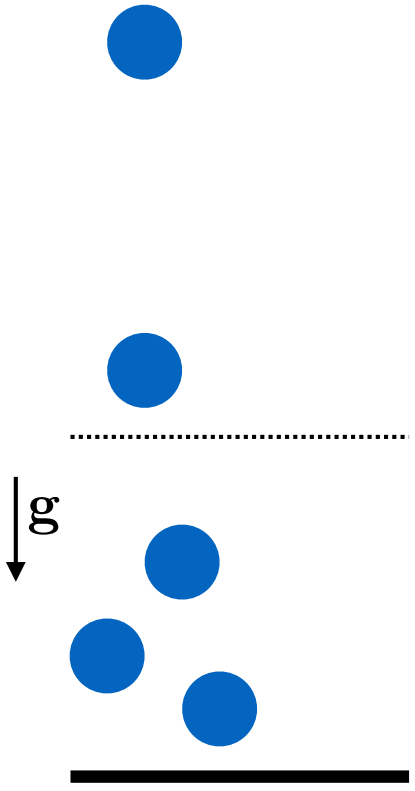

$$\langle V \rangle = F_{\text{sed}} b_0 K(\phi)$$
$$= \frac{4}{3}\pi a^3 \Delta\rho g \frac{1}{6\pi\eta a} K(\phi)$$
$$= V K(\phi)$$

$$j_{\text{sed}} = -\phi\langle V \rangle$$

$$j_{\text{diff}} = -D_c(\phi)\nabla\phi$$

$$D_c = D_0 K(\phi)\frac{d}{d\phi}[\phi Z(\phi)]$$

$$Z = \Pi / nkT$$

osmotic compressibility

Sedimentation coefficient

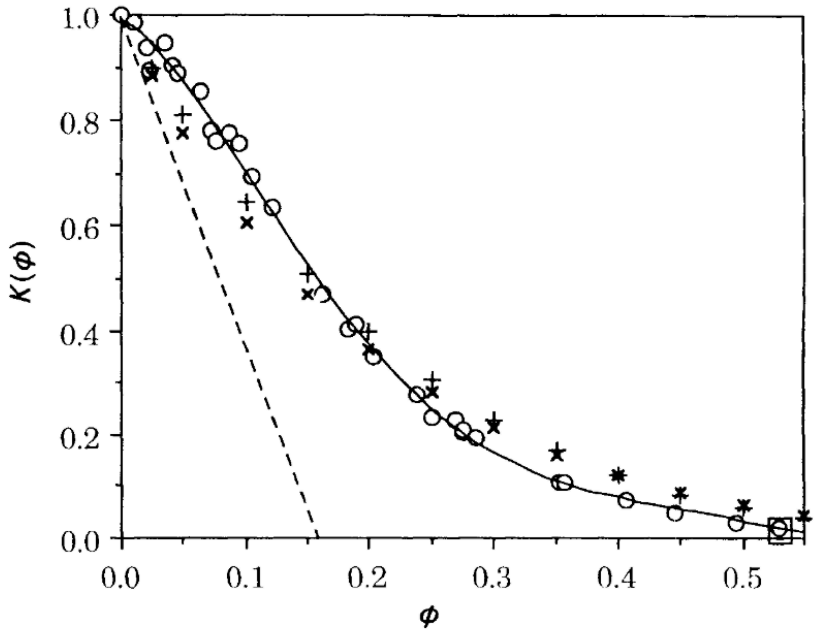

Fig. 2 The dimensionless sedimentation coefficient. The circles are experimental values calculated with data from batches 11, 12 and 13 (0.28, 0.31 and 0.27 μm, respectively). The solid curve denotes the polynomial fit of these data, (——) $0.99159 - 1.367\phi - 23.930\phi^2 + 106.30\phi^3 - 167.22\phi^4 + 91.985\phi^5$. Also shown are the predictions of Brady and Durlofsky[37] (×), Garside and Al-Dibouni[38] (+) and Batchelor's hard-sphere limit[36] (– – –)

Higher concentrations

Particle concentration (osmotic pressure) and hydrodynamic interactions (settling dynamics and diffusion) will play a role

Davis, K. E.; Russel, W. B. *J. Chem. Soc. Faraday Trans.* 1991, 87, 411–424.
Davis, K. E.; Russel, W. B. *Phys. Fluids A Fluid Dyn.* 1989, 82, 82–100.

$$j_{\mathrm{tot}} = j_{\mathrm{sed}} + j_{\mathrm{diff}}$$

$$\frac{\partial \phi}{\partial t} + \frac{\partial j_{\mathrm{tot}}}{\partial x} = 0$$

$$\frac{\partial \phi}{\partial t} - V\frac{\partial}{\partial x}\phi K(\phi) = D_0\frac{\partial}{\partial x}\left(K(\phi)\frac{d}{d\phi}[\phi Z(\phi)]\right)$$

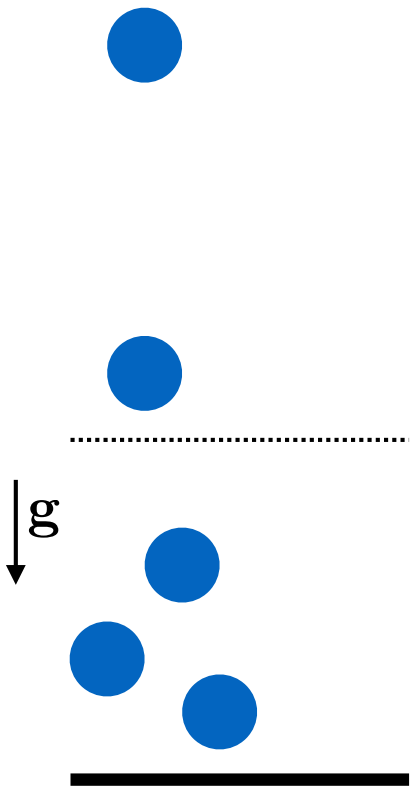

$$j_{\mathrm{tot}}(x = 0, h_0) = 0 \qquad \phi = \phi_0 \ \text{ at } \ t = 0$$

In a scaled, non-dimensional form,

$$\frac{\partial \phi}{\partial t'} - \frac{\partial}{\partial x'}\phi K(\phi) = \frac{1}{\mathrm{Pe}}\frac{\partial}{\partial x'}\left(K(\phi)\frac{d}{d\phi}[\phi Z(\phi)]\right) \qquad \mathrm{Pe} = \frac{V h_0}{D_0}$$

$$x' = x/h_0 \qquad t' = tV/h_0$$

Numerical solutions

Davis, K. E.; Russel, W. B. *Phys. Fluids A Fluid Dyn.* 1989, 82, 82–100.

$\mathrm{Pe} = 100$

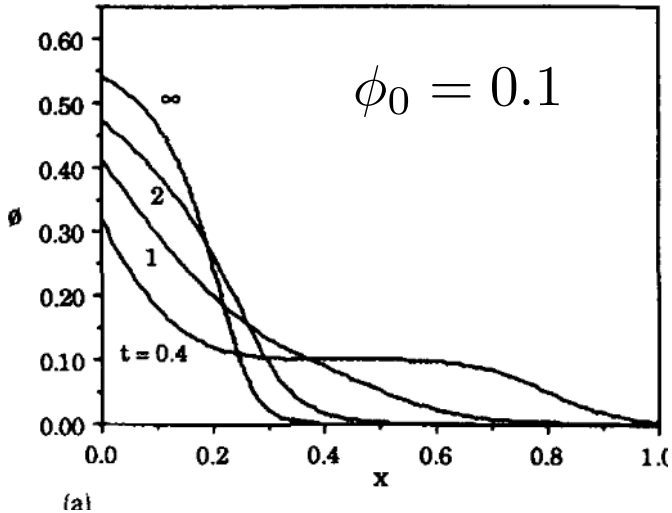

$\mathrm{Pe} = 10^3$

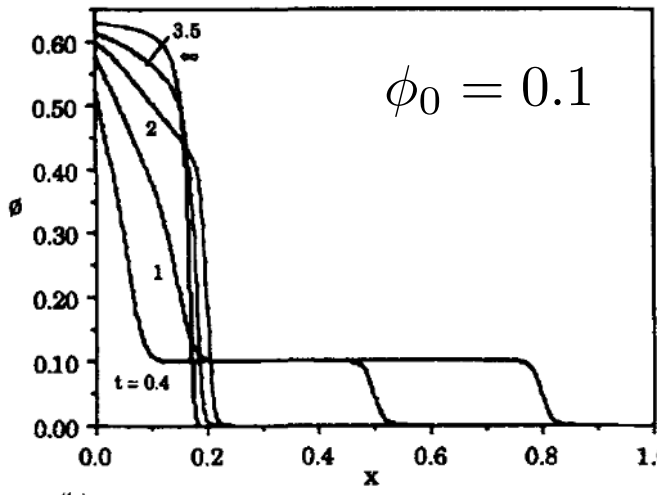

$\mathrm{Pe} = 10^4$

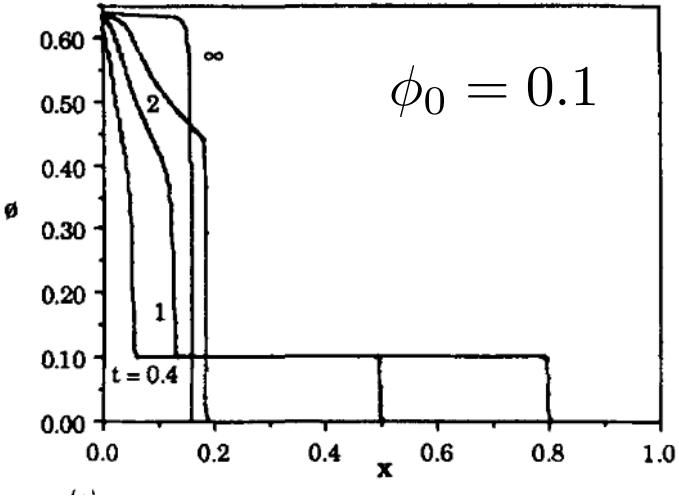

steady state

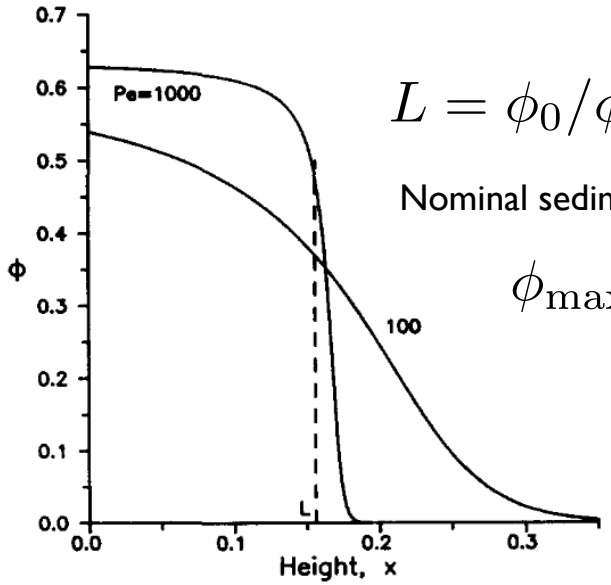

$L = \phi_0/\phi_{\max}$

Nominal sediment height

$\phi_{\max} \approx 0.64$

$x' = x/h_0$

When $\mathrm{Pe}(x' - L) \gg 1$

$$\phi(x') \sim \phi_{\max} \exp[-(\phi_{\max}/c)\mathrm{Pe}(x' - L)]$$

$$c = 1.85$$

Iron oxide settling behavior

G. G. Glasrud, R. C. Navarrete, L. E. Scriven, C. W. Macosko, Settling Behaviors of Iron Oxide Suspensions. AIChE J. 39, 560–568 (1993).

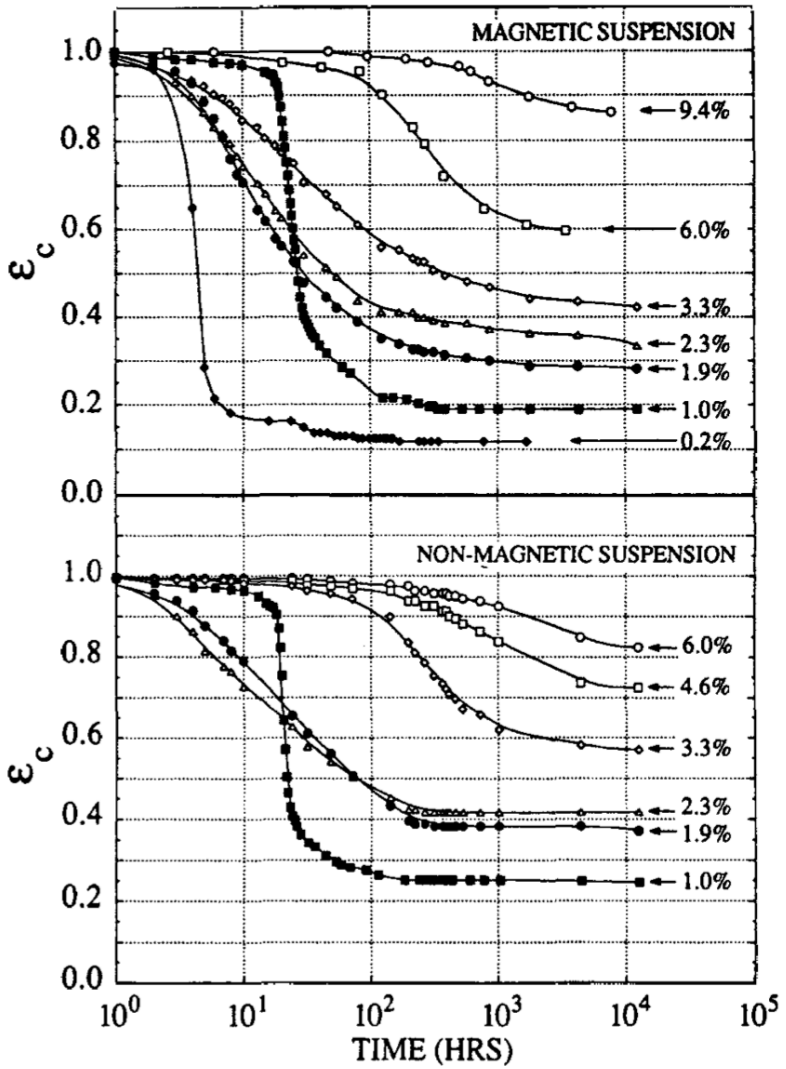

Figure 1. Settling curves of Fe_2O_3 suspensions of indicated concentrations.

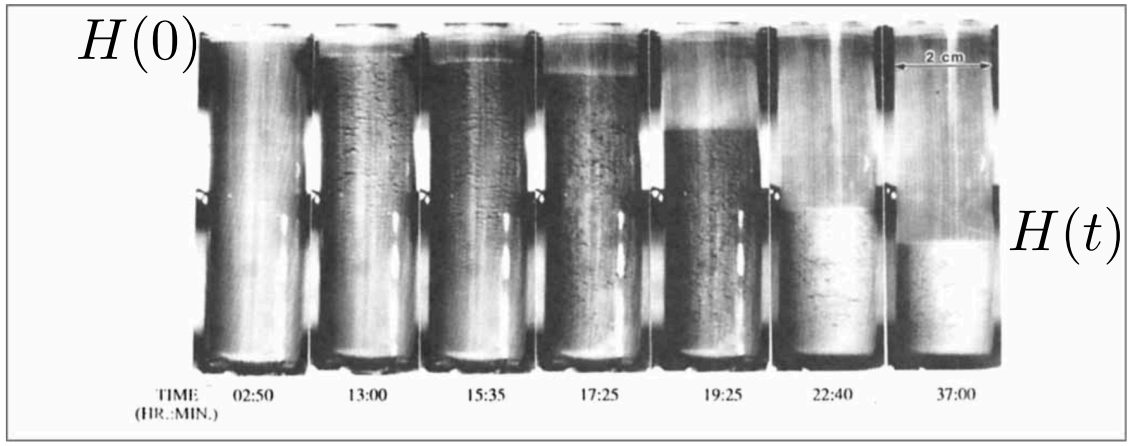

Figure 2. Side-by-side time-lapse photographs of the settling of a 1.0% by volume magnetic iron oxide suspension.

- 500nm needle-like iron oxide (Fe_2O_3) a*nisotropic, polydisperse*
- Attraction leads to denser sediments and faster settling
- Horizontal cracking
- Rising air bubbles create channels

Compressive strain $\epsilon_c = H(t)/H(0)$

Attraction – faster settling, more compact sediment

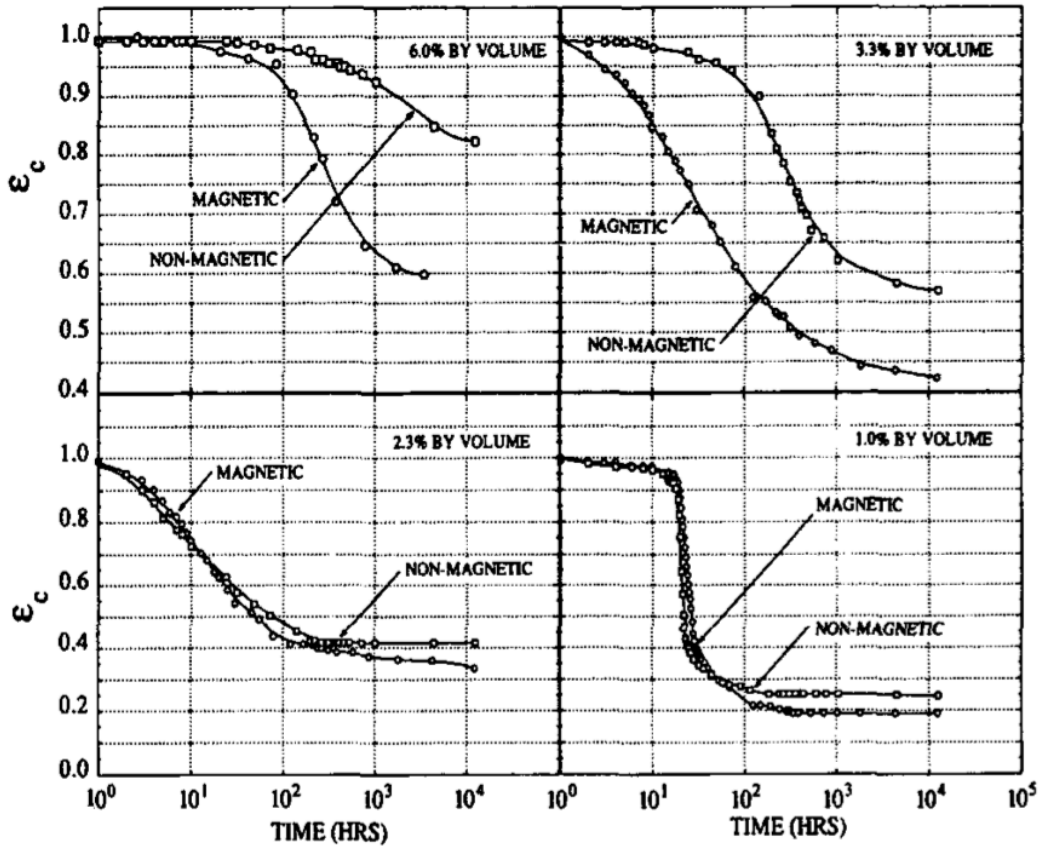

Figure 4. Comparison between magnetic and nonmagnetic Fe_2O_3 settling curves.

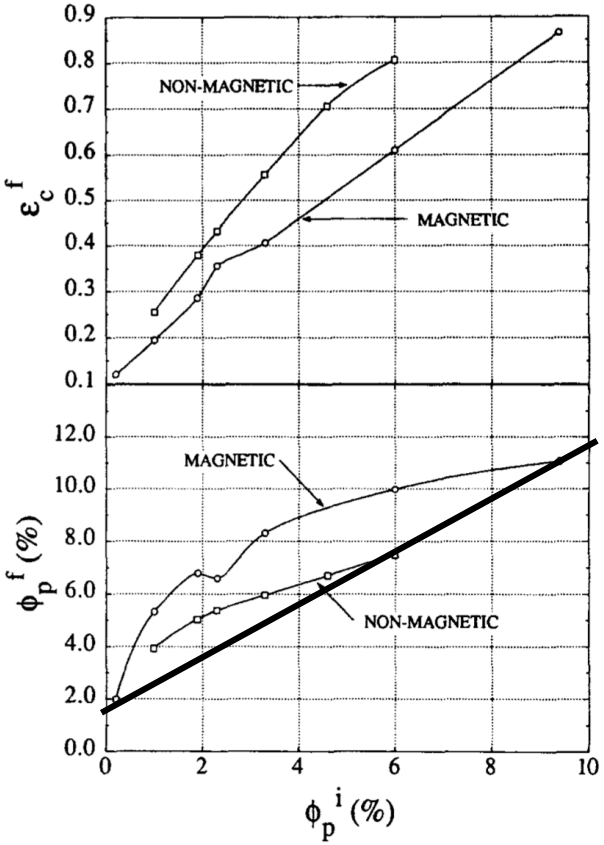

Figure 13. Comparison of final compressive strain and final particle volume fraction vs. initial particle volume fraction between magnetic and nonmagnetic iron oxide suspensions.

Final sediment volume fraction $\phi_p^f = \dfrac{\phi_p^i}{\epsilon_c^f}$

G. G. Glasrud, R. C. Navarrete, L. E. Scriven, C.W. Macosko, AIChE J. 39, 560–568 (1993).

Smaller diameter containers delay settling

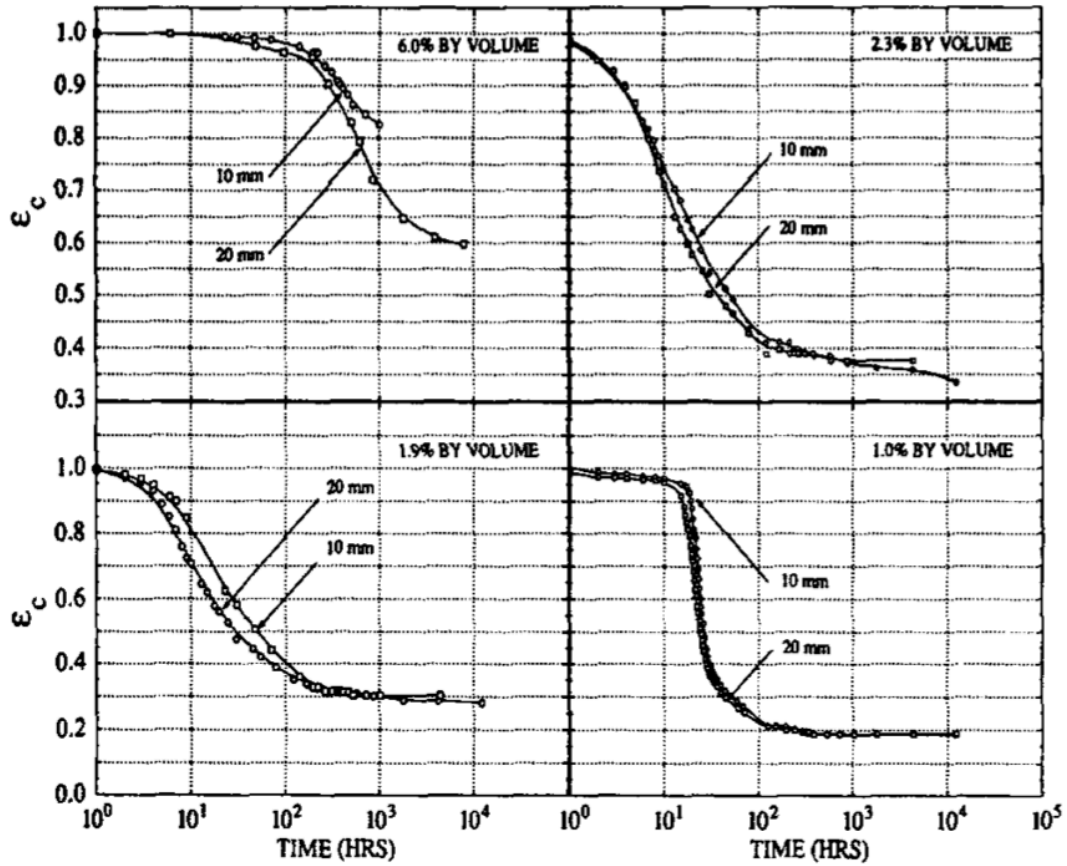

Figure 5. Effect of test tube diameter on settling curves of γ-Fe_2O_3 suspensions of indicated particle volume fractions.

Wall shear stress and shear-thinning?

G. G. Glasrud, R. C. Navarrete, L. E. Scriven, C.W. Macosko, AIChE J. 39, 560–568 (1993).

Rising air bubbles create channels for solvent back flow

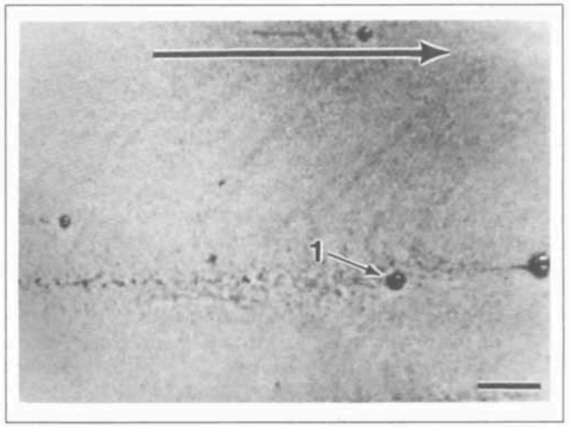

Figure 6. Air bubble ascending through a just loaded 1.0% by volume γ-Fe_2O_3 suspension (1).
Arrow indicates vertical direction. (Bar = 0.5 mm).

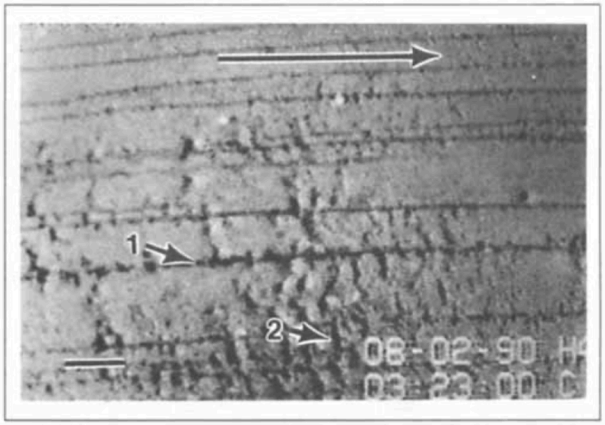

Figure 7. Paths created by ascending air bubbles (1) through a 1.0% by volume γ-Fe_2O_3 suspension before collapse at indicated time.
Horizontal cracks created between bubble paths (2). Arrow indicates vertical direction. (Bar = 0.5 mm).

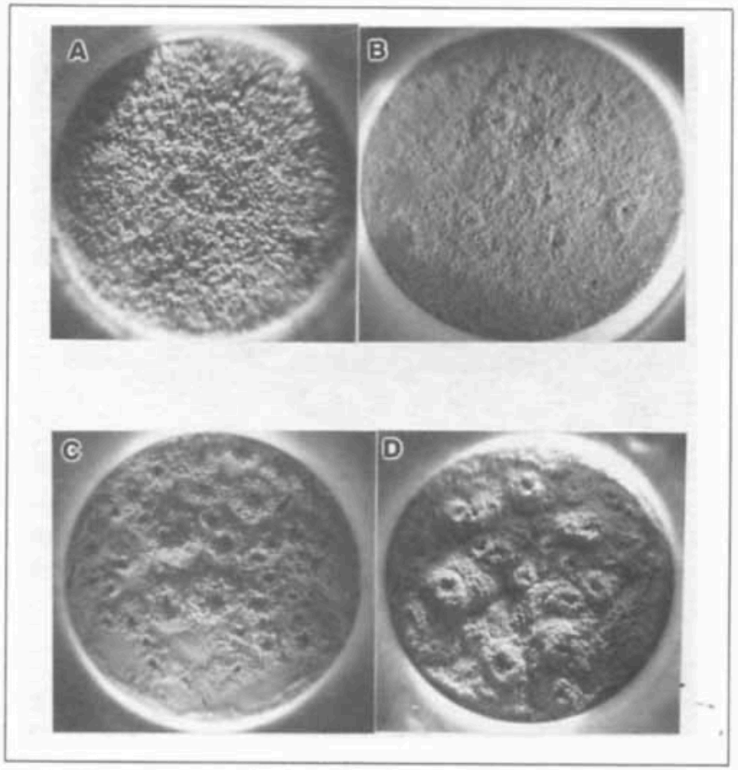

Figure 9. Top view of test tubes after about 1,500 h of settling of Fe_2O_3 suspensions (tube diameters are all 20 mm).
(A) and (C) are 1.0% and 2.3% magnetic respectively; (B) and (D) are 1.0% and 2.3% nonmagnetic respectively.

Vesicle dispersion creaming

J.Y. Huh, M. L. Lynch, E. M. Furst, Microscopic structure and collapse of depletion-induced gels in vesicle-polymer mixtures. Phys. Rev. E. 76, 51409 (2007).

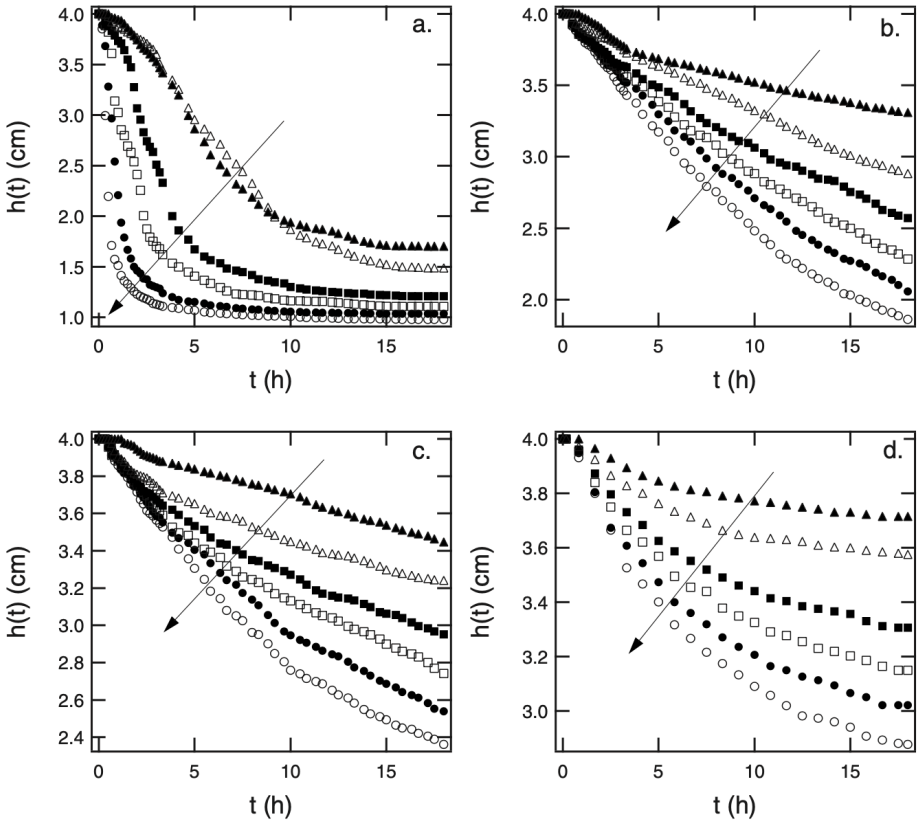

FIG. 4. Time evolution of the height as a function of polymer concentration for $R_g/a \approx 0.09$ at (a) $\phi=0.05$, (b) $\phi=0.15$, (c) $\phi=0.2$, and (d) $\phi=0.3$ for $C_P=0.3$ wt % (solid triangles), $C_P=0.6$ wt % (open triangles), $C_P=0.9$ wt % (solid squares), $C_P=1.2$ wt % (open squares), $C_P=1.6$ wt % (solid circles), and $C_P=2.0$ wt % (open circles). The arrow indicates the increase in polymer concentration from 0.3 to 2.0 wt%.

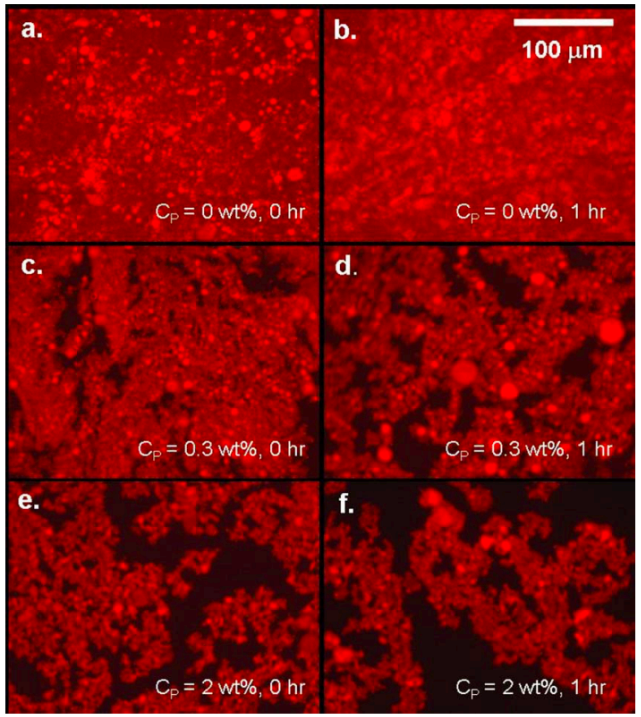

FIG. 7. (Color online) Short time-evolution in microstructure measured by fluorescence microscopy at $\phi=0.3$ and $R_g/a \approx 0.09$ immediately after sample preparation (a) $C_P=0$ wt %, (b) $C_P=0.3$ wt %, and (c) $C_P=2.0$ wt %; 1 h after sample preparation (d) $C_P=0$ wt %, (e) $C_P=0.3$ wt %, and (f) $C_P=2.0$ wt %. Vesicles are stained red.

Attraction leads to faster settling (creaming) due to increasing porosity of microstructure, which enables faster solvent back-flow

Initial settling velocity

R. Buscall, L. R. White, The Consolidation of Concentrated Suspensions. J. Chem Soc. Faraday Trans. 83, 873–891 (1987).

$$\left.\frac{dH}{dt}\right|_0 = -\frac{(1-\phi_0)u_0}{r(\phi_0)}\left[1-\frac{1}{B}\right] \qquad B > 1$$

$$\left.\frac{dH}{dt}\right|_0 = 0 \qquad B < 1$$

$$B = \frac{\Delta\rho g \phi_0 H_0}{P_y(\phi_0)} \longleftarrow \frac{\text{gravitational stress}}{\text{compressive yield stress}}$$

$$u_0 = \frac{2a^2\Delta\rho g}{9\eta_s} \longleftarrow \text{settling velocity of single sphere}$$

Hydrodynamic interactions

$$r(\phi_0) \to \infty,\ \phi_0 \to 1 \qquad r(\phi_0) \sim a^2/k(\phi_0)$$

$$r(\phi_0) \to 1,\ \phi_0 \to 0 \qquad k_0 = 0.022a^2\frac{(1-\phi_0)^3}{\phi_0^2}$$

Carman-Kozeny permeability

Compressive yield stress

Buscall, R. et al. "The rheology of strongly-flocculated suspensions." J. Non-Newtonian Fluid Mech. 24, 183–202 (1987).

Polystyrene latex in salt solutions

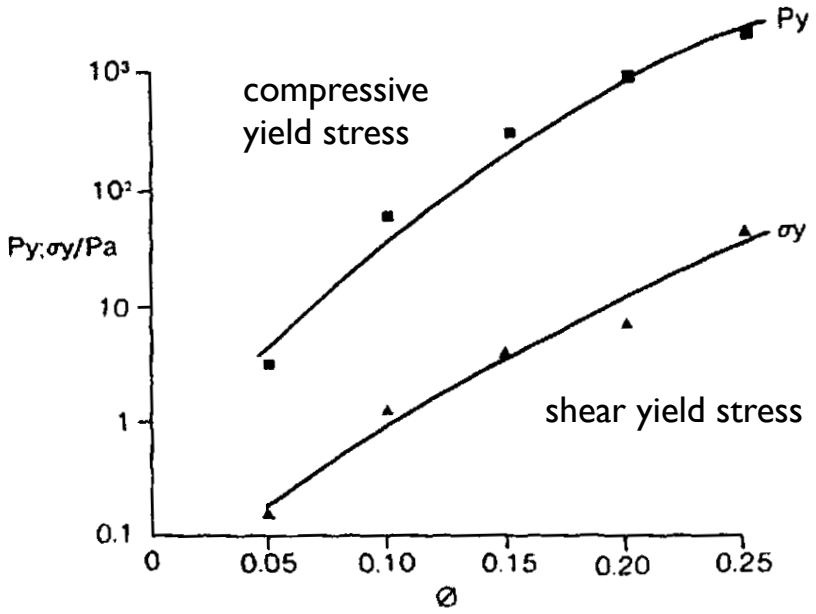

$$P_y \propto G \propto \phi^x$$

$$x \sim 4.0 - 5.0$$

Compression — dewatering and filtration

Initially low compressive yield stress

Solve for the permeability

$$k_0 \approx -\frac{a^2}{(1-\phi_0)u_0}\left.\frac{dH}{dt}\right|_0$$

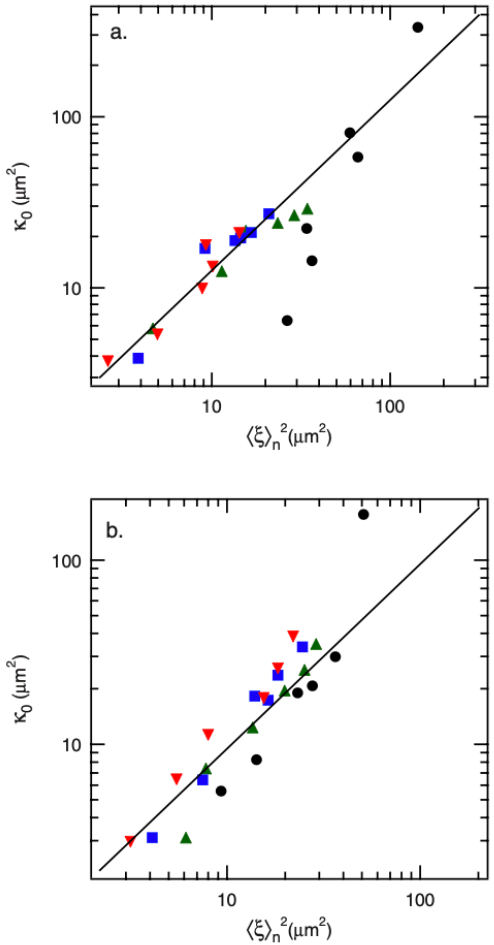

Permeability ~ microstructure pore size

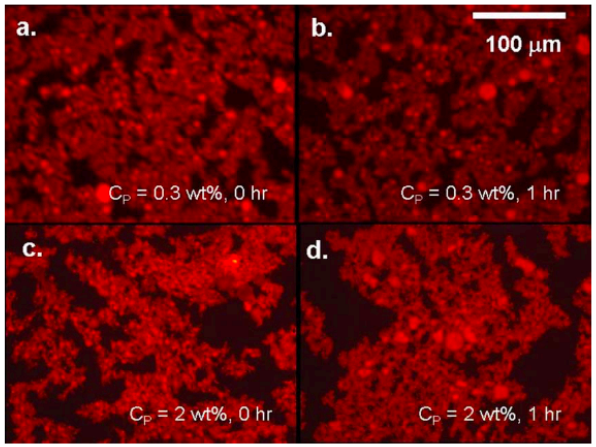

$$k_0 \sim \xi^2$$

FIG. 10. (Color online) The characteristic pore area $\langle\xi\rangle_n^2$ shows the similar dependence on both polymer concentration and vesicle volume fraction to the initial permeability k_0: ϕ=0.05 (black circles), ϕ=0.15 (green upper triangles), ϕ=0.2 (blue squares), and ϕ=0.3 (red lower triangles) for (a) $R_g/a \approx 0.09$ and (b) $R_g/a \approx 0.27$. The line has a slope of 1 for comparison.

Monodisperse silica in CMC

M. L. Kilfoil, E. E. Pashkovski, J. A. Masters, D. A. Weitz, Dynamics of weakly aggregated colloidal particles. Phil. Trans. R. Soc. A. 361, 753–766 (2003).

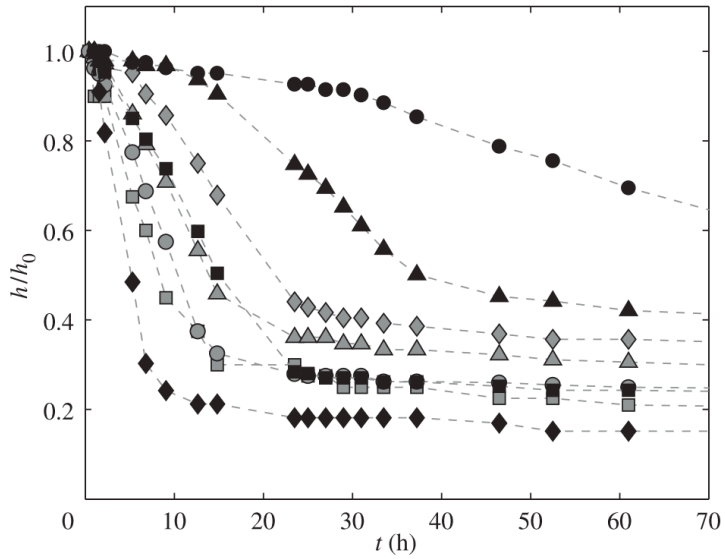

Figure 1. Sedimentation profiles for 0.5 μm silica/CMC/glycerol/water colloid–polymer mixtures at $\phi = 0.11$: black diamond, $C_p = 0.087$ wt%; black square, $C_p = 0.16$ wt%; black circle, $C_p = 0.25$ wt%; grey square, $C_p = 0.33$ wt%; grey triangle, $C_p = 0.5$ wt%; grey diamond, $C_p = 0.75$ wt%; black triangle, $C_p = 1.0$ wt%; black circle, $C_p = 1.5$ wt%. To account for slightly different initial heights, the height, $h(t)$, has been normalized by the initial height, h_0, for each profile. The profiles show the characteristic delay before collapse of the colloidal network.

Note with increasing attraction:
longer induction
less dense sediment

Scaled master curve

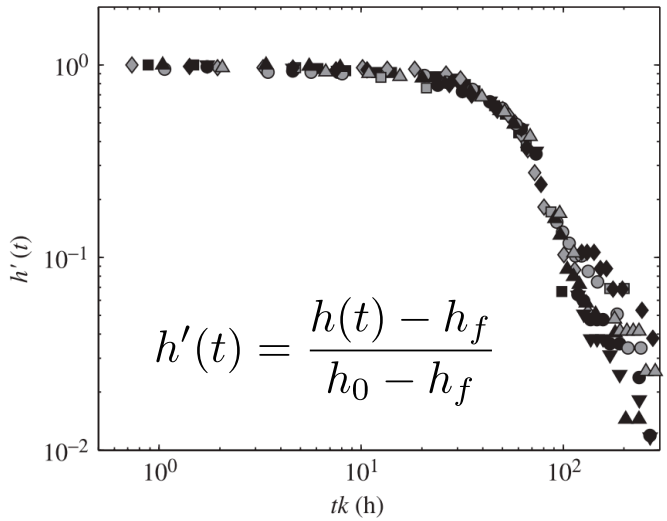

Figure 3. Master curve showing the normalized profiles as a function of scaled time for all data in figure 1, at $\phi = 0.11$ and varying polymer concentration C_p. The scale factors yield the delay time τ for the onset of the collapse for each polymer concentration.

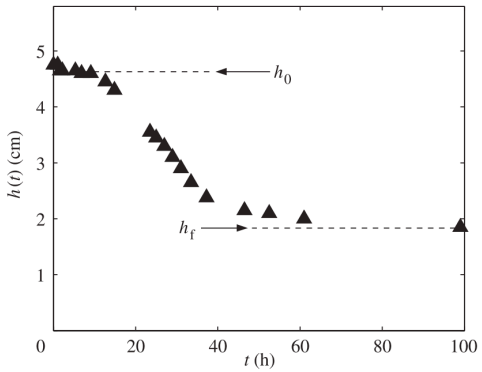

initial and
final height

Monodisperse silica in CMC

M. L. Kilfoil, E. E. Pashkovski, J. A. Masters, D. A. Weitz, Phil. Trans. R. Soc. A. 361, 753–766 (2003).

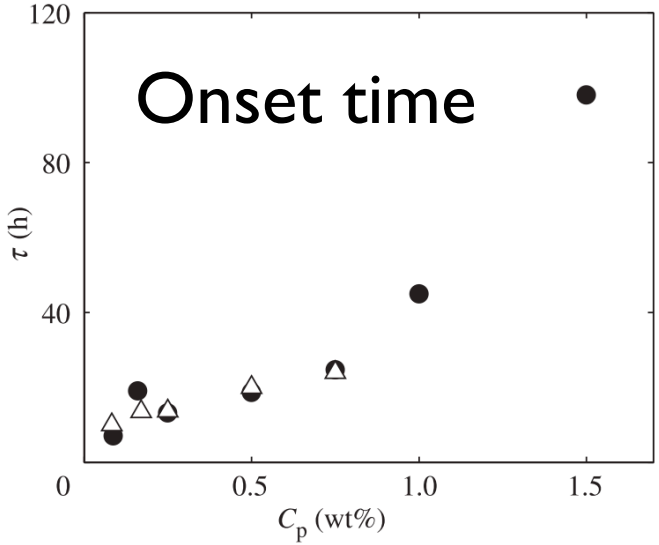

Figure 4. Dependence of onset time for the delayed collapse on C for $\phi = 0.11$ (solid symbols) and $\phi = 0.055$ (open symbols).

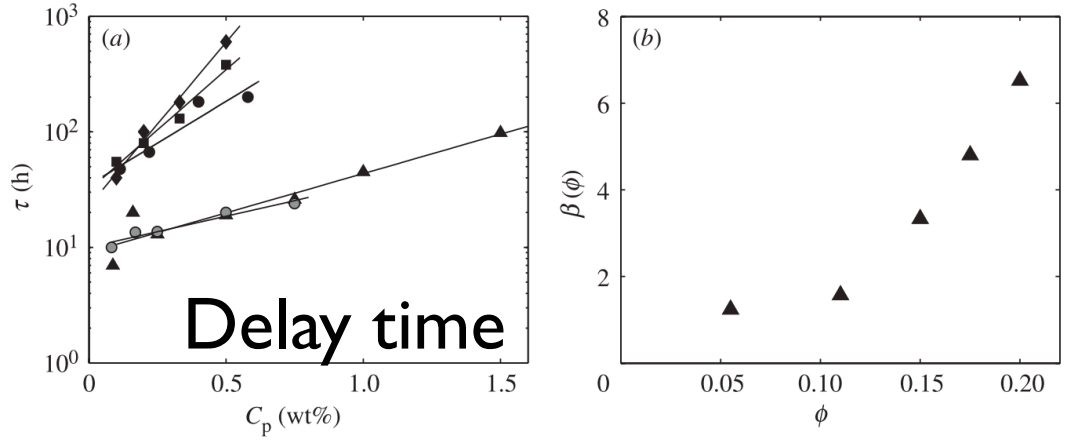

Figure 5. (*a*) Dependence of the delay time, τ, determined from the scaling, on polymer concentration for different ϕ; when the delay times are plotted logarithmically in time as a function of C_p, all of the data for each ϕ fall onto a straight line. Grey circle, $\phi = 0.055$; black triangle, $\phi = 0.11$; black circle, $\phi = 0.15$; black square, $\phi = 0.175$; black diamond, $\phi = 0.20$. (*b*) Exponential dependence, β, plotted as a function of ϕ; $\beta(\phi)$ is nearly independent of ϕ for $\phi \leqslant 0.10$, and it increases roughly linearly with ϕ for $\phi > 0.10$.

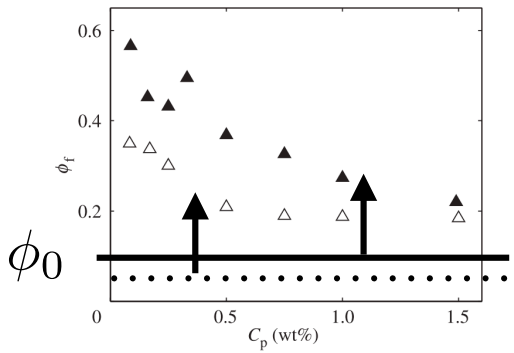

Final sediment volume fraction

Figure 6. Comparison of final colloid volume fraction, ϕ_f, of the collapsed state for starting volume fractions, $\phi = 0.11$ (solid symbols) and $\phi = 0.055$ (open symbols). ϕ_f decreases as C_p is increased. The final state is more collapsed for starting volume fraction $\phi_i = 0.11$ than for $\phi_i = 0.055$, with ϕ_f approaching 0.20 at high polymer concentration in both cases.

Monodisperse PMMA with PS depletant

L. Starrs, W. C. K. Poon, D. J. Hibberd, M. M. Robins, Collapse of transient gels in colloid-polymer mixtures. J. Phys. Condens. Matter. 14, 2485–2505 (2002).

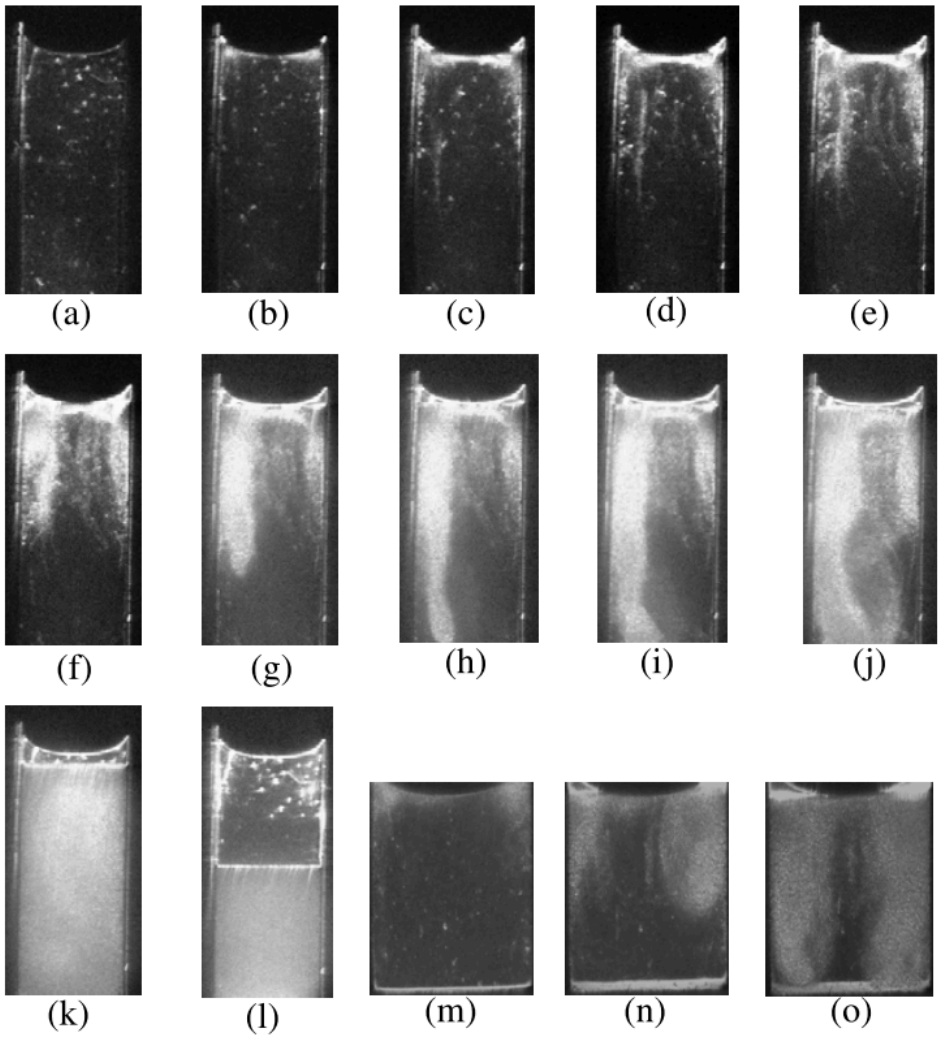

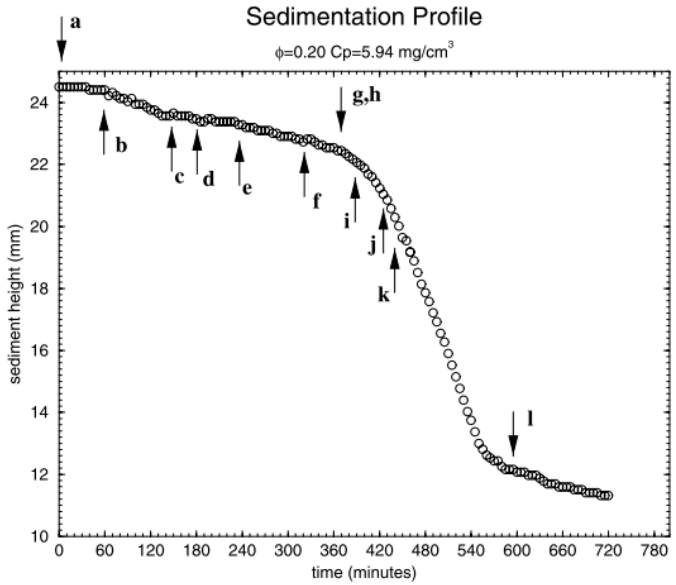

Figure 4. Dark-field images of a gel undergoing delayed sedimentation with a latency time of 420 min. For images (*a*)–(*l*) the time at which each image was captured is shown in the $h(t)$ plot for this sample. Images (*m*)–(*o*) show what happens at the bottom of a sample during delayed sedimentation. Here the latency time was 200 min and the images were captured at 60, 150 and 180 min respectively. An animated GIF of this figure is available (2.5 MB).

Delayed sedimentation

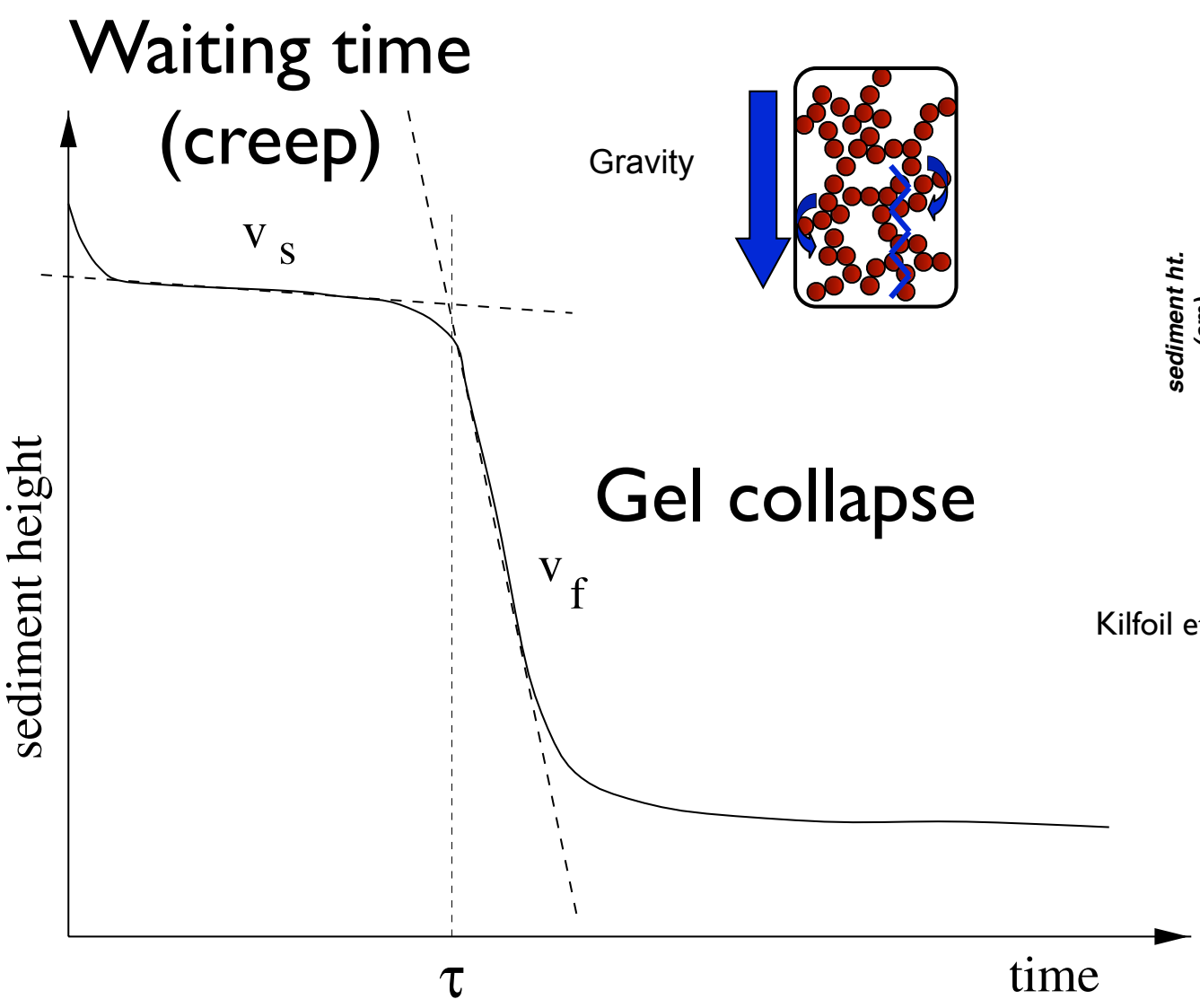

L. Starrs, et al. J. Phys. Condens. Matter, 14:2485–2505, 2002.

Gopalakrishnan et al., J. Phys.: Condens. Matter 18, 11531 (2006).

0.55 μm silica/ decalin/ PS

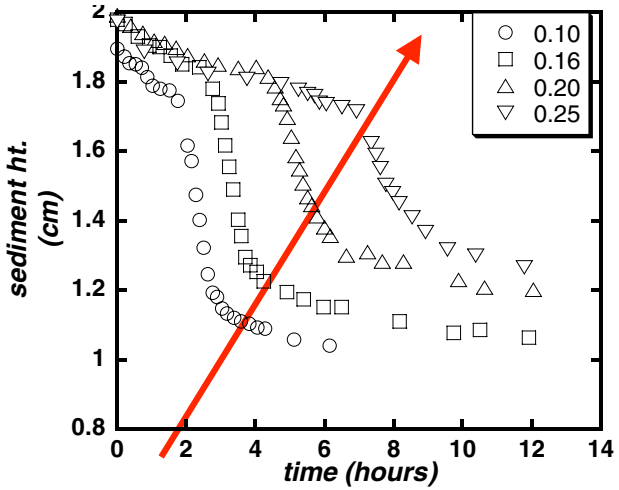

Kilfoil et al., Phil. Trans. R. Soc. Lond. A 361, 753 (2003)

0.5 μm silica / CMC / glycerol / water

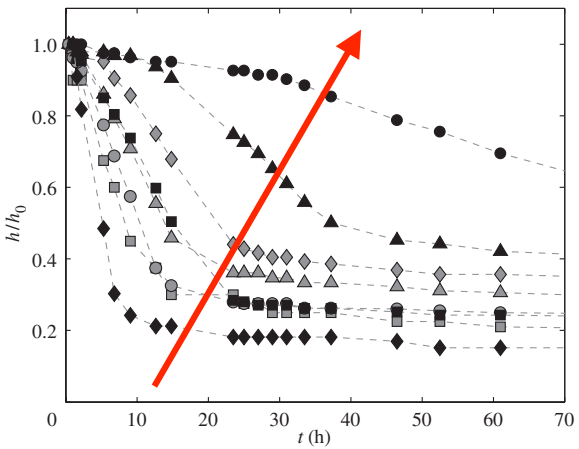

Increasing attraction

Model of delayed collapse

Zs. Varga, J. L. Hofmann, J. W. Swan, J. Fluid Mech. 856, 1014–1044 (2018).

Settling and solvent backflow

Pore nucleation

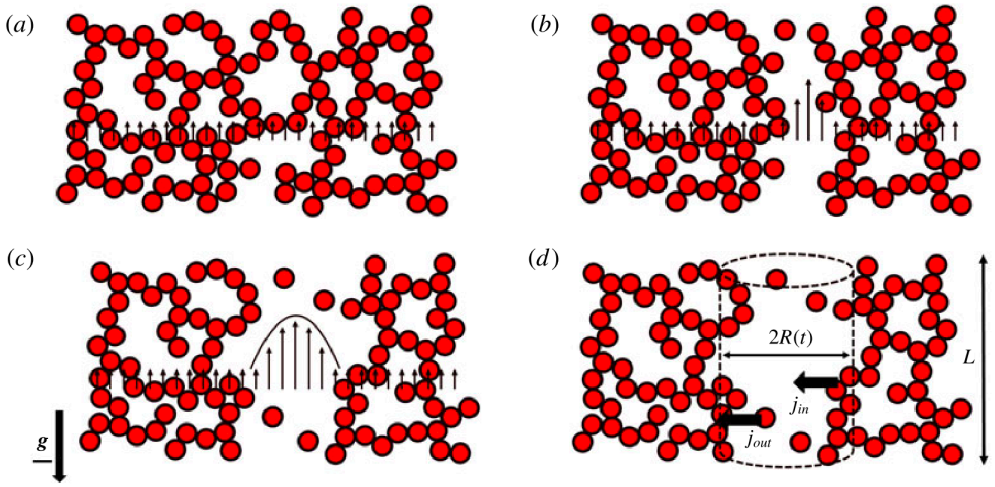

Erosion and growth